I. Hattabi, A. Abdiche*, R. Moussa, R. Riane, K. Hadji, F. Soyalp, Dinesh Varshney, S.V. Syrotyuk and R. Khenata

First-Principle Study of the Structural, Electronic, and Optical Properties of Cubic InN_xP_{1-x} Ternary Alloys under Hydrostatic Pressure

DOI 10.1515/zna-2016-0100

Received March 16, 2016; accepted July 8, 2016; previously published online August 5, 2016

Abstract: In this article, we present results of the first-principle study of the structural, electronic, and optical properties of the InN, InP binary compounds and their related ternary alloy InN_vP_{1-v} in the zinc-blend (ZB) phase within a nonrelativistic full potential linearised augmented plan wave (FP-LAPW) method using Wien2k code based on the density functional theory (DFT). Different approximations of exchange-correlation energy were used for the calculation of the lattice constant, bulk modulus, and firstorder pressure derivative of the bulk modulus. Whereas the lattice constant decreases with increasing nitride composition x. Our results present a good agreement with theoretical and experimental data. The electronic band structures calculated using Tran-Blaha-modified Becke-Johnson (TB-mBJ) approach present a direct band gap semiconductor character for InN₂P₁ compounds at different x values. The electronic properties were also

*Corresponding author: A. Abdiche, Applied Materials Laboratory, Research Center, University of Sidi-bel-Abbes, 22000 Sidi-bel-Abbes, Algeria, Tel.: +213 05 60 62 40 49, E-mail: abdiche_a@yahoo.fr

I. Hattabi: Laboratoire Synthèse et Catalyse, Ibn Khaldoun Université de Tiaret, Postbox78-Zaaroura, 14000 Tiaret, Algeria R. Moussa: Physic Department, University of Sidi-bel-Abbes, Sidibel-Abbes 22000, Algeria

R. Riane: Applied Materials Laboratory, Research Center, University of Sidi-bel-Abbes, 22000 Sidi-bel-Abbes, Algeria

K. Hadji: Science and Technology Département Ibn Khaldoun Université de Tiaret, Postbox78-Zaaroura, 14000 Tiaret, Algeria F. Soyalp: Yüzüncü Yıl University, Faculty of Education, Department of Physics, Van 65080, Turkey

Dinesh Varshney: Materials Science Laboratory, School of Physics, Vigyan Bhavan, Devi Ahilya University, Khandwa Road Campus, Indore 452001, India

S.V. Syrotyuk: Semiconductor Electronics Department, National University "Lviv Polytechnic", S. Bandera str. 12, Lviv 79013, Ukraine
R. Khenata: Laboratoire de Physique Quantique et de Modélisation Mathématique (LPQ3M), Département de Technologie, Université de Mascara, 29000 Mascara, Algerie

calculated under hydrostatic pressure for (P=0.00, 5.00, 10.0, 15.0, 20.0, 25.0 GPa) where it is found that the InP compound change from direct to indirect band gap at the pressure $P \ge 7.80$ GPa. Furthermore, the pressure effect on the dielectric function and the refractive index was carried out. Results obtained in our calculations present a good agreement with available theoretical reports and experimental data.

Keywords: Band Gap; InN_xP_{1-x} ; Optical Properties; Pressure Effect; Semiconductor.

1 Introduction

Semiconductor compounds are the basis materials for different fields of technologies, as well as new classes of optoelectronic devices. Some examples include high electron mobility and transistors, heterostructures, light-emitting diodes, photodetectors, and modulators.

The InN and InP compounds are interesting semiconductors materials for high-frequency electronic devices, by reason of its superior speed electrons. These alloys have undergone a variety of experimental and theoretical studies. Recently, in experimental study, the electronic structure of InP was studied by Lev et al. [1]. Aspnes and Studna measured the dielectric function of III-V semiconductors of InP and obtained more other optical constants in the energy range 1.5-6.0 eV [2]. Besides, the dielectric constants of InP compound between 0.7 and 5.0 eV including a band gap around 1.42 eV measured by Herzinger et al. [3]. The direct band gap of high-quality wurtzite InN films is reported [4, 5] to be from 0.65 to 1 eV. The band gap of the cubic InN is foreseen to be within this range or slightly lower. This allows manufacturing the highspeed LDs and PDs for optical communication systems [4]. On the other hand, some results for structural and electronic properties were reported by Boussahla et al. [6], as well as Ben Fredj et al. [7, 8]. The strong dependence of the band gap on the N content has made diluted III-V

nitrides important materials for a variety of applications, including long wavelength optoelectronic devices [9, 10] and high-efficiency hybrid solar cells [11, 12]. Several theoretical studies of band structure calculations using density functional theory (DFT) have addressed the unusually strong dependence of the fundamental gap on the N content in the group III-N-V alloys [13, 14]. Recently, structural and electronic properties of InN_vP_{1-v} alloys were investigated in full range (0 < x < 1) by Aslan et al. [15].

Some of the III-V compounds, in particular the InP, InN, and their ternary InN P_{1-x} solid solutions form crystals with zinc blende arrangement, which is based on the cubic space group $F\overline{4}3m$ in which the lattice parameter obeys to the Vegard's law and varies linearly with the composition *x* of nitrogen [16].

Here, we investigate the structural, electronic, and optical properties of the cubic InN and InP binary compounds together with their related ternary InN, P, solid solutions using the first-principles calculations by perthe Tran-Blaha-modified, Becke-Johnson forming (TB-mBI) approach band structure calculations. The electronic and optical properties were also carried out under hydrostatic pressure effect. The calculations were made by applying a nonrelativistic full potential linearised augmented plane waves (FP-LAPW) method in the context of the DFT as implemented in the Wien2k package [17].

2 Computational Details

Calculations were performed using DFT because of the efficiency of this approach for different systems. For periodic systems, we have gathered an extensive experience with the all-electron full-potential linearised plane wave (FP-LAPW)-based code Wien2k [18]. This code uses "forces" to optimise the crystal structure. The periodical calculations of properties, at the k-space through the Fourier transformations techniques, employed in expansions of both the electronic wave functions and the potential generated by the nucleus.

The exchange-correlation potential was treated within the generalised gradient approximation (WC-GGA). In addition to this approximation, the (local density approximation, LDA) and (PBE-sol GGA) was also applied for computing structural properties such as the lattice

Table 1: The lattice constants (a), bulk modulus (B), and pressure derivative of the bulk modulus (B') for the InN, InP, and the zinc blende $InN_x P_{1-x}$ alloys.

Composition x	Parameters			This work	Other theoretical	Experimental data
		WC-GGA	PBEsol-GGA	PW-LDA	studies	
InN	a (Å)	4.9926	4.9918	4.9471	4.945°, 4.98°	4.98 ^f
	B (GPa)	140.5343	137.2588	145.5469	145°, 155.35b	137e
	B'	4.1757	3.7960	3.6884	4.75°, 4.49b	
InN _{0.75} P _{0.25}	a (Å)	5.2638	5.2624	5.2131		
	B (GPa)	103.3437	103.0356	111.7882		
	B'	4.7490	4.3744	4.7623		
$InN_{0.5}P_{0.5}$	a (Å)	5.5052	5.5036	5.4525		
	<i>B</i> (GPa)	84.1868	83.7418	92.0391		
	B'	4.5969	4.1304	4.3859		
$InN_{0.25}P_{0.75}$	a (Å)	5.7105	5.7087	5.6579		
0.25 0.75	<i>B</i> (GPa)	73.0259	72.8655	78.5801		
	B'	4.3392	4.5467	4.6981		
InP	a (Å)	5.8814	5.8789	5.8299	5.72 ^d , 5.85 ^g	5.86 ^d
	B (GPa)	67.7383	67.2997	71.0719	73.66 ^d , 76.10 ^h	72.00 ^d
	B'	4.3041	4.5021	4.6221	4.20i	4.80 ⁱ

aRef. [21].

^bRef. [22].

cRef. [23].

dRef. [7].

eRef. [24].

fRef. [25].

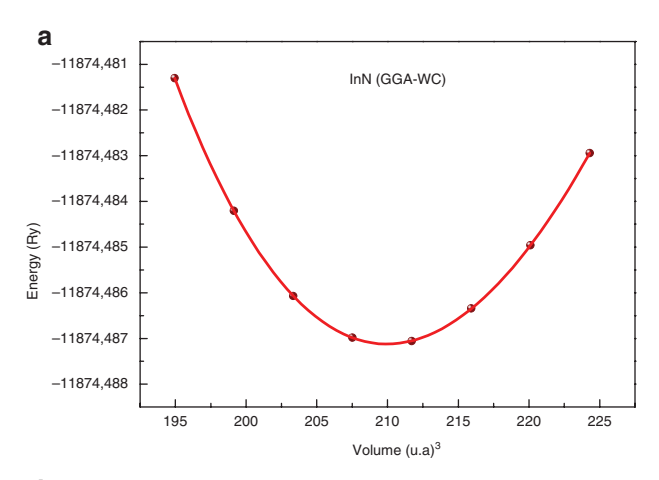
gRef. [26].

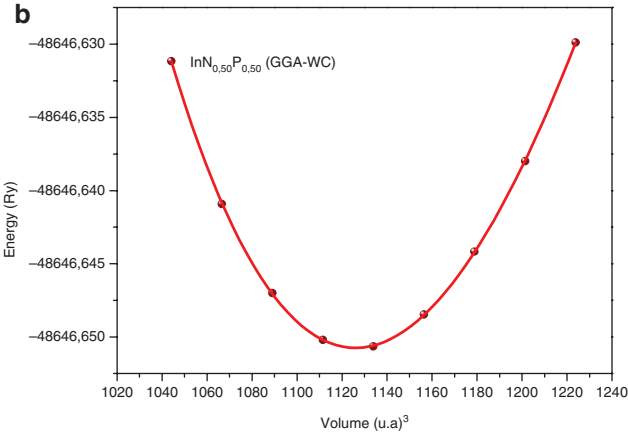
hRef. [8].

Ref. [27].

constants, bulk modulus, and their pressure derivatives. The obtained results were fitted using the Birch–Murnaghan's equation of state [19].

In order to model the InN_xP_{1-x} alloys with different compositions x = 0.0, 0.25, 0.5, 0.75, and 1.0, we have used a cubic cell $1 \times 1 \times 1$ with eight atoms. For each configuration, the band gap energy, the dielectric constants, and





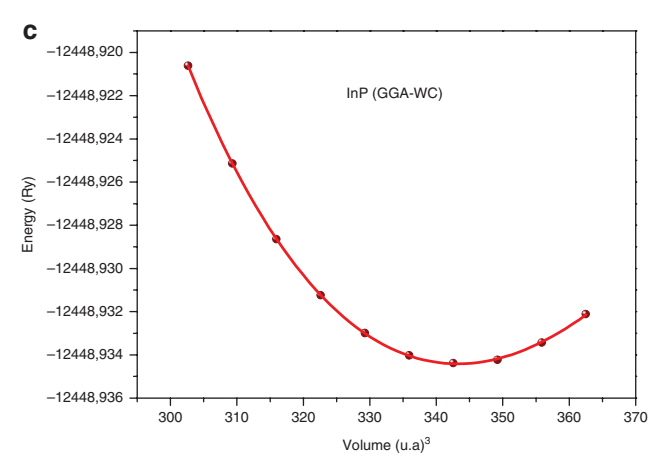


Figure 1: Energy versus volume curves of (a) InN, (c) InP, and (b) $InN_{0.5}P_{0.5}$ compounds for WC-GGA exchange—correlation energy approximations.

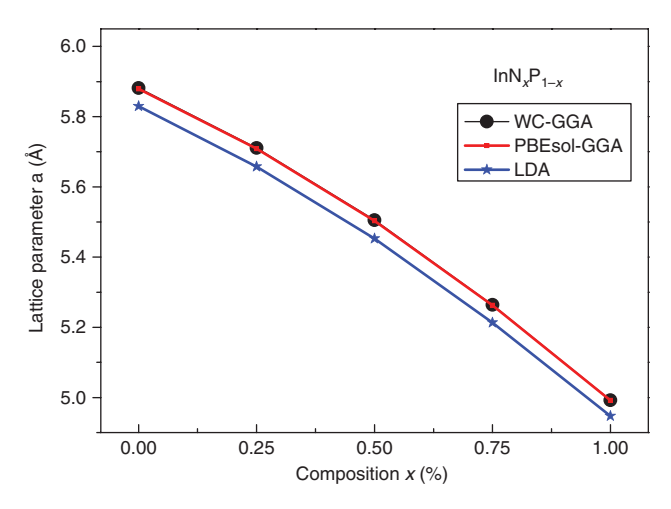


Figure 2: Variation of the lattice constant versus composition, x, of the (ZB) InN,P, $_{-x}$ alloy.

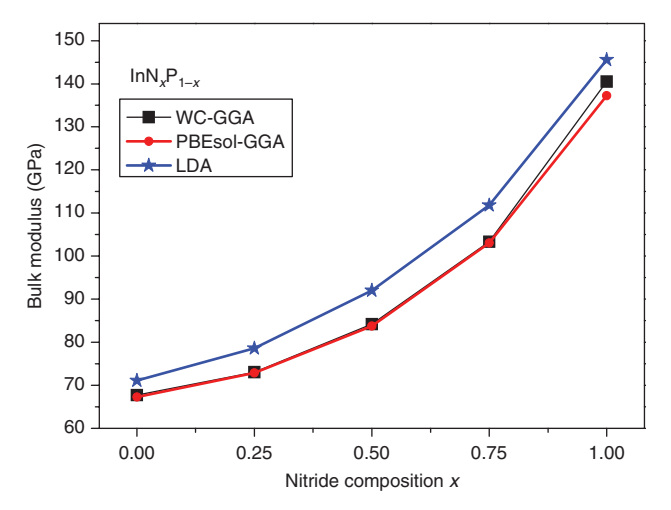


Figure 3: Variation of the bulk modulus versus composition, x, of the (ZB) InN_xP_{1-x} alloy.

the refractive index were studied under hydrostatic pressure effect for different values of pressure (P=0, 5, 10, 15, 20, 25 GPa). The matrix size was defined with a parameter $R_{\rm mt} \times K_{\rm max}$ equal to 8, where the $R_{\rm mt}$ denotes the minimum radius of the sphere in unit cell, and $K_{\rm max}$ yields the extent of the largest K vector in the plane wave expansion. The muffin-tin radii of In, N, and P are adopted to be 2.1, 1.4, and 1.7 Bohr, respectively. We have chosen a value of -6.0 Ry for the energy cutoff between the core and the valence states for both compounds, we have fixed $l_{\rm max}$ =10 for wave function expansion inside the atomic spheres and the charge density was Fourier expanded up to $G_{\rm max}$ =12 (Ryd). The integrals over the Brillouin zone are performed up to 47 k-points, the energy convergence was selected as 0.0001 Ry.

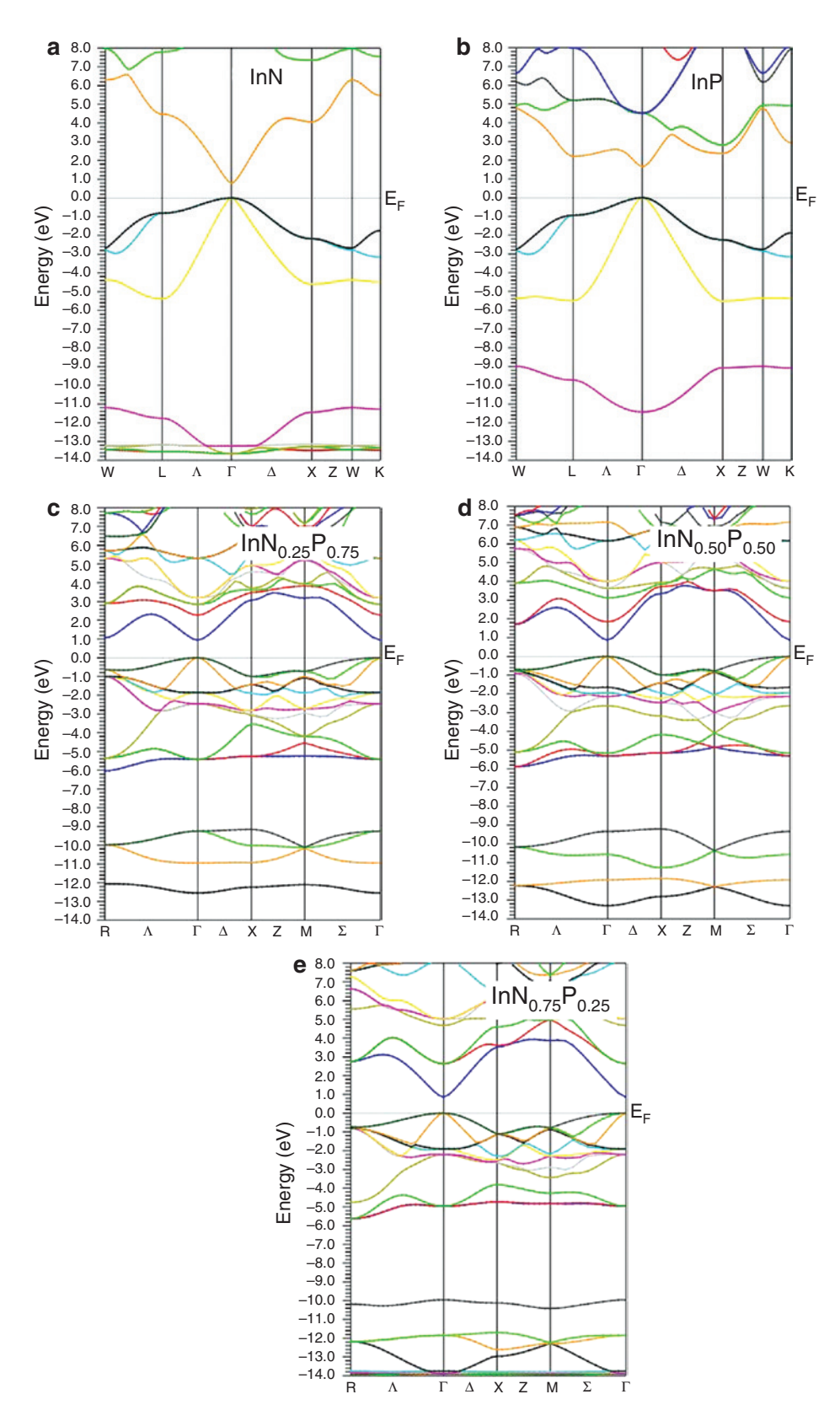


Figure 4: (a, b) The electronic band structures of the cubic (a) InN and (b) InP alloys within TB-mBJ approximation. The electronic band structures tures of the cubic (c) $InN_{0.25}P_{0.75}$, (d) $InN_{0.5}P_{0.5}$ and (e) $InN_{0.75}P_{0.25}$ alloys within TB-mBJ approximation.

Table 2: The band gap energies of the direct and indirect transitions of the InN, P, compounds for the compositions (x = 0.00, 0.25, 0.50,0.75, and 1.00), where the values are given in electron volts.

Composition	Band gap	This work	Other theoretical	Experimental	
x at P atom	energy (eV)	LDA_mBJ	studies	data	
InN	$E_{\Gamma ightarrow \Gamma}$	0.79110	0:69ª	0.7 ^b	
	$egin{aligned} E_{\Gamma ightarrow X} \end{aligned}$	4.06859	2.765°	2:11 ^d	
$InN_{0.75}P_{0.25}$	$E_{\Gamma o \Gamma}$	0.86179			
0.7,5 0.2,5	$E_{\Gamma o X}$	3.52952			
$InN_{0.5}P_{0.5}$	$E_{\Gamma o \Gamma}$	0.87223			
	$E_{\Gamma o X}$	3.35265			
$InN_{0.25}P_{0.75}$	${\cal E}_{\Gamma o\Gamma}$	0.94014			
0.25 0.75	$E_{\Gamma \to X}$	3.07013			
InP	$E_{\Gamma o \Gamma}$	1.66753	1.423°	1.35 ^f	
	$E_{\Gamma o X}$	2.36479	1.63 ^g	2.21 ^f	

aRef. [30].

The band structures were calculated using the TB-mBJ approach with the parameterisation of Koller et al. [20]. The total and partial densities of states (DOSs) were calculated. We have to note that for the DOS calculations, we have used a denser k-mesh of 3000 k-points and we have distinguished the In $(1s^2 2s^2 2p^6 3s^2 3p^6 3d^{10} 4s^2 4p^6)$, N $(1s^2)$, and P (1s² 2s² 2p⁶) as inner-shell electrons from the valence electrons of In $(4d^{10} 5s^2 5p^1)$, N $(2s^2 2p^3)$, and P $(3s^2 3p^3)$ shells.

3 Results and Discussion

3.1 Structural Properties

The lattice constants (a), bulk modulus (B), and pressure derivatives of the bulk modulus (B') at the corresponding volumes of cubic InN_xP_{1-x} alloys using the LDA, WC-GGA, and PBEsol-GGA approximations, for different compositions (x = 0.00, 0.25, 0.50, 0.75, 1.00), are computed. Results obtained are summarised in Table 1, together with available measured values and other theoretical available data. Our calculated lattice constants are very close to those given in the literature. We show as a prototype in Figure 1 the variation of total energy as a function of volume by fitting the total energies to the Murnaghan's equation of state [19].

The difference can be observed between the lattice parameter value of InP (x = 0, $a_0 = 5.88 \text{ Å}$) compound, and

these of the InN (x=1, $a_0=4.99$ Å) can be explained by the difference in the atomic radius of the P(0.98 Å) atom from that of the atom N(0.65 Å), which allows us to note that the decrease in lattice parameter of the InN, P, ternary compounds have an inversely relationship with increasing x composition. In opposition to the lattice constant a_0 and in concordance with the proportionality between the Bulk modulus and the lattice constants: $B\alpha V_0^{-1}$ [28], the bulk modulus increases with increasing x composition. The calculated equilibrium lattice constants of InN_xP_{1-x} alloys are plotted as a function of x composition in Figure 2. We

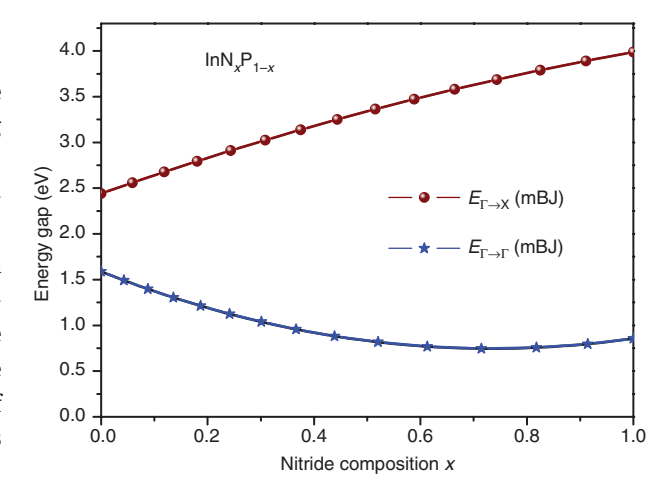


Figure 5: The variations curves versus composition x of each band gap $(E_{\Gamma \to \Gamma}, E_{\Gamma \to X})$ of the $InN_x P_{1-x}$ alloys.

^bRef. [25].

cRef. [22].

dRef. [31].

eRef. [32].

fRef. [33]. ^gRef. [27].

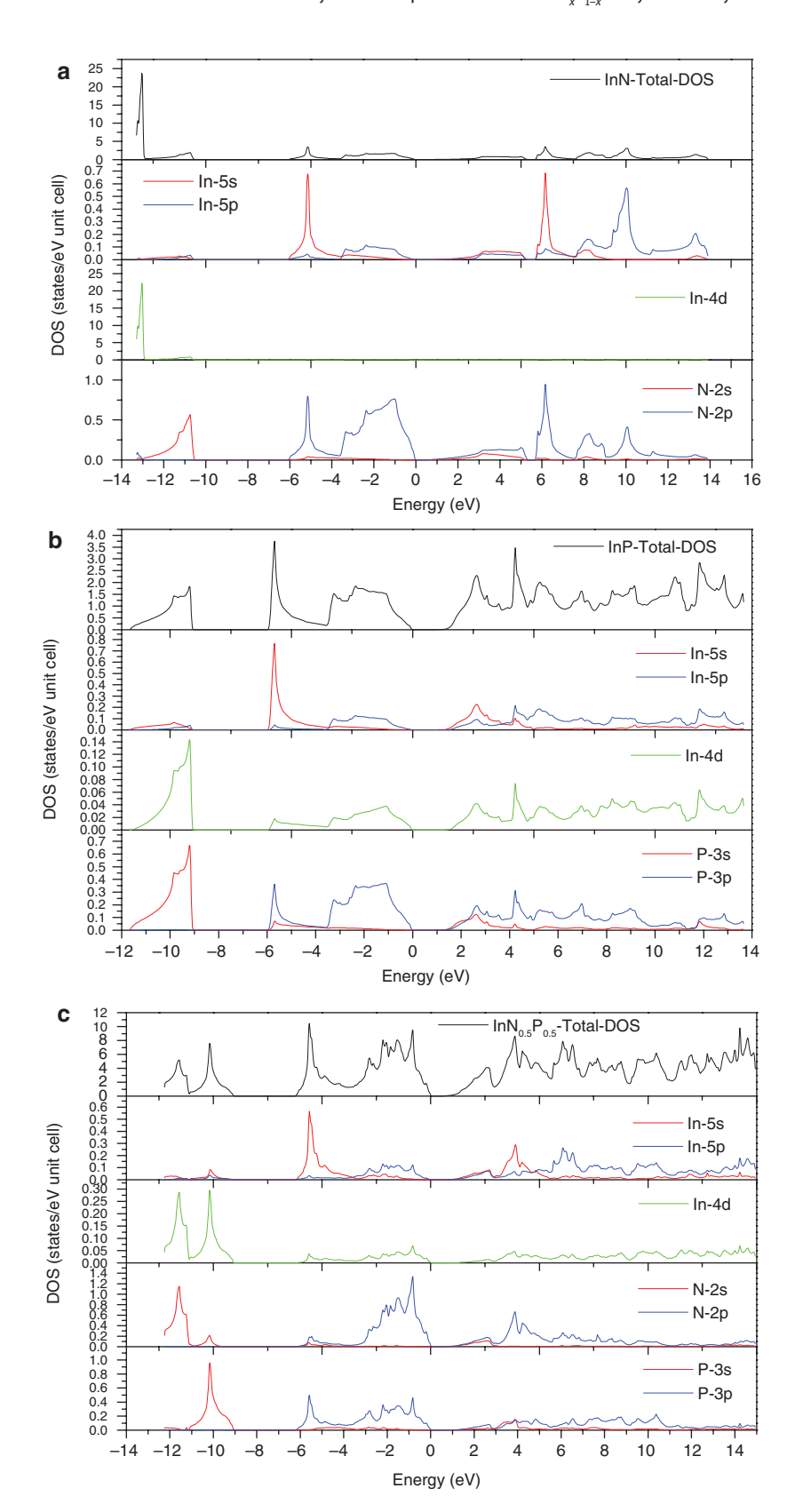


Figure 6: The total and partial density of states for the (a) InN, (b) InP, and (c) $InN_{0.5}P_{0.5}$ alloys.

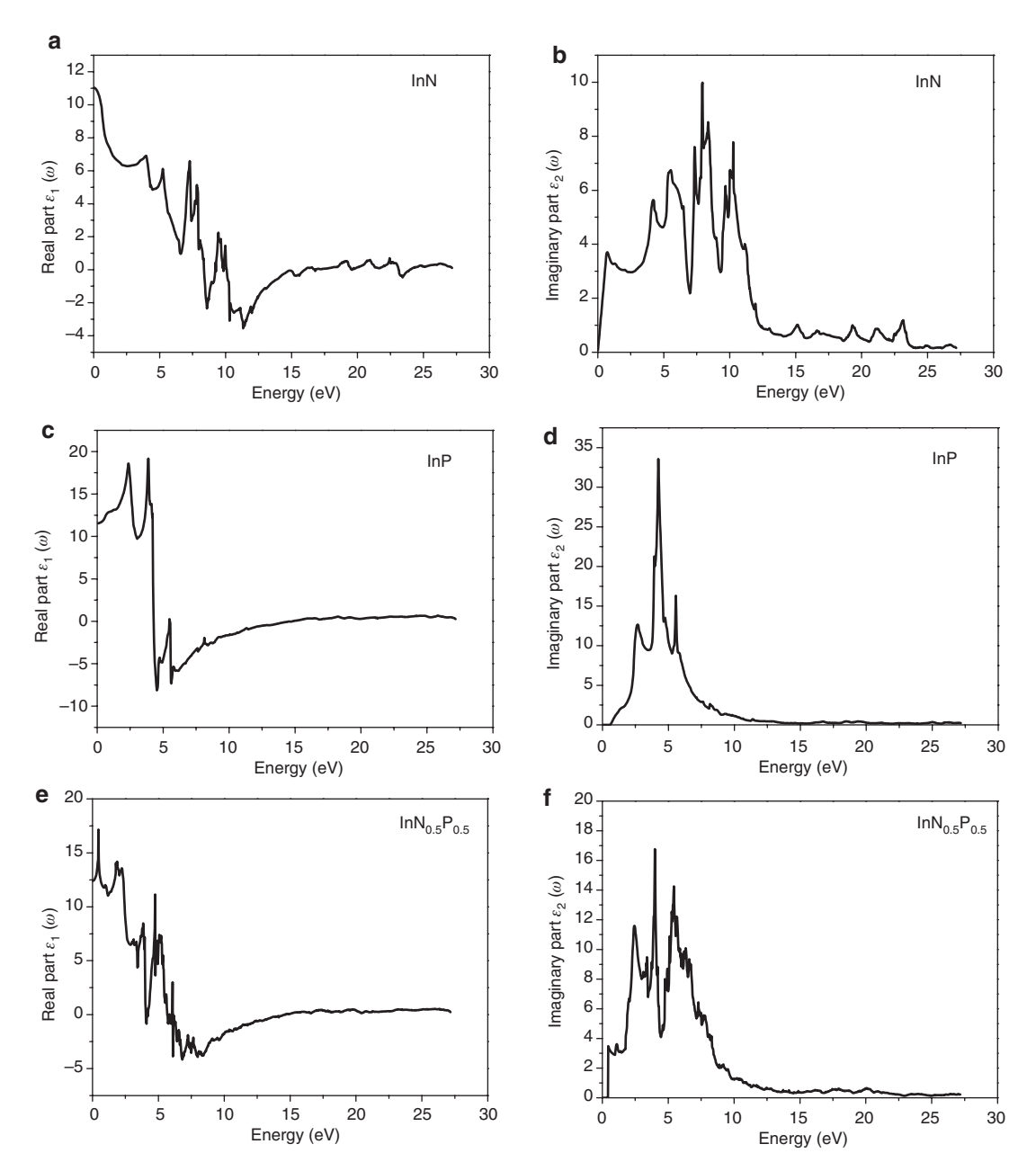


Figure 7: The real and imaginary parts of the dielectric function of the (ZB) (a, b) InN, (c, d) InP, and (e, f) InN $_{0.5}$ P $_{0.5}$ alloys.

Table 3: The refractive index *n* of the InN_xP_{1-x} compounds (x = 0.00, 0.50, 1.00).

Compound	FP-LAPW $n(\omega=0)$	Herve–Vandam $n(\omega=0)$	Ravindran $n(\omega=0)$	Reddy $n(\omega=0)$	Moss $n(\omega=0)$	Kumarn (ω=0)	Other works $n(\omega=0)$
InN	3.32	3.39	3.59	3.83	3.31	3.63	2.92ª
$InN_{0.5}P_{0.5}$	3.52	3.34	3.55	3.74	3.24	3.53	_
InP	3.39	2.86	3.15	3.08	2.75	2.85	3.32b

aRef. [40].

^bRef. [41].

can observe a slight deviation from the Vegard's law [29], the physical origin of this deviation should be mainly due to the difference in atomic radii and the lattice mismatch between binary compounds InP an InN which is at about 15.11%. A quadratic polynomial function is used to fit the calculated values of the structural properties. The fit function is given as fellow:

$$a(x)=xa_{_{\text{InN}}}+(1-x)a_{_{\text{InP}}}-x(1-x)b$$
 (1)

The bowing parameters of the lattice constants curves are found to be equal to -0.27051, -0.27074, and -0.25371 for the WC-GGA, PBEsol-GGA, and PW-LDAs, respectively.

With the same scheme, we have calculated the bowing parameter of the bulk modulus for InN_xP_{1-x} , solid solutions. Values are 82.0594, 75.1226, and 67.1898 for the WC-GGA, PBEsol-GGA, and PW-LDA approaches, respectively. The bulk modulus versus composition x for the InN_xP_{1-x} alloys are depicted in Figure 3. Unfortunately, we have not found any report in literature for more comparison of our results for the ternary alloys InN_xP_{1-x} .

3.2 Electronic Structure

In this section, the energy band structures and the density of states DOS are investigated for both binary constituents InP, InN, and their related ternary alloys $\mathrm{InN}_x\mathrm{P}_{\mathrm{I-x}}$. For a wide range of materials, standard DFT calculations using modern approximations as well as the generalised gradient approach (GGA), the local density LDA, and other approximations give extremely useful results in structural properties calculations, but it is known that they underestimate dramatically the band gaps of most semiconductors and leads to incorrect prediction comparing with experimental results. In this regard, we have introduced the Tran–Blaha-modified Becke Johnson (TB-mBJ) approach in our calculations. The TB-mBJ approximation gives a very much improved band gaps for a large variety of materials including semiconductors.

In this approach, the TB-mBJ potential is given by

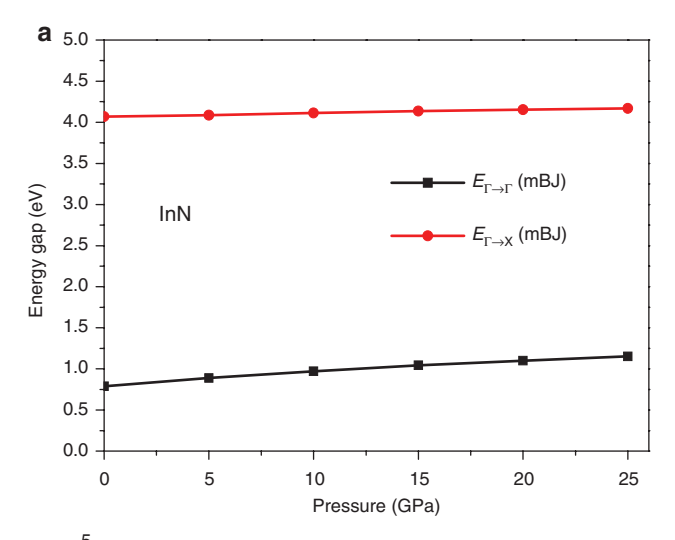
$$v_x^{\text{TB-mBJ}}(r) = cv_x^{BR}(r) + (3c - 2)\frac{1}{\pi}\sqrt{\frac{5}{12}\sqrt{\frac{2t(r)}{\rho(r)}}}$$
 (2)

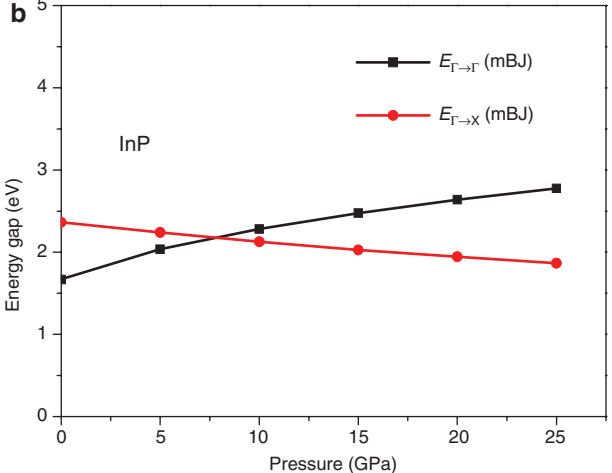
where c is given by

$$c = A + B\sqrt{g'}$$

$$g' = \frac{1}{V_{\text{cell}}} \int_{\text{cell}} \frac{1}{2} \left(\frac{\left| \nabla \rho \uparrow(r) \right|}{\rho \uparrow(r)} + \frac{\left| \nabla \rho \downarrow(r) \right|}{\rho \downarrow(r)} \right)$$
(3)

where g' is the average of $g=|\nabla\rho|/\rho$ in the unit cell of volume V_{cell} . According to a fit to the experimental values of band gaps, A and B parameters values are A=-0.012 and B=1.023 bohr^{1/2}.





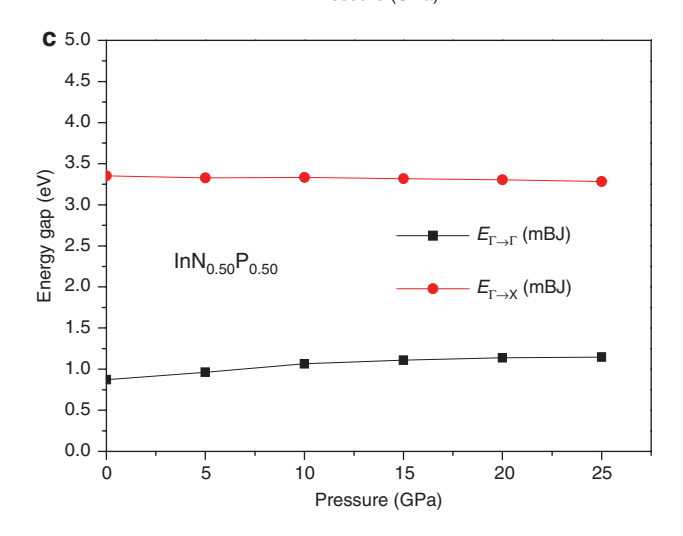


Figure 8: The direct and indirect band gaps energies versus pressure of (a) InN, (b) InP, and (c) $InN_{0.5}P_{0.5}$ alloys.

1.86804

2.12825

Composition <i>x</i> at P atom	Band gap energy (eV)					Hydrostatic pressure P (GPa)	
		0	5	10	15	20	25
InN	${\it E}_{_{\Gamma ightarrow \Gamma}}$	0.79110	0.88842	0.97088	1.04396	1.10098	1.15155
	$E_{\Gamma \to X}$	4.06859	4.08692	4.11275	4.13811	4.15406	4.17004
$InN_{0.75}P_{0.25}$	$E_{\Gamma o \Gamma}$	0.86179	0.98163	1.07573	1.15816	1.22139	1.27984
0.75 0.25	$E_{\Gamma \to X}$	3.52952	3.61036	3.67263	3.72586	3.76517	3.80134
$InN_{0.5}P_{0.5}$	$E_{\Gamma \to \Gamma}$	0.87223	0.96123	1.06396	1.10902	1.13676	1.14807
0.5 0.5	$E_{\Gamma \to X}$	3.35265	3.32565	3.33382	3.31844	3.30200	3.28279
$InN_{0.25}P_{0.75}$	$E_{\Gamma \to \Gamma}$	0.94014	0.98412	0.97020	0.92748	0.87693	0.82095
0.25 0.75	$E_{\Gamma \to X}$	3.07013	3.02893	2.98615	2.94030	2.89729	2.85431
InP	$E_{\Gamma \to \Gamma}$	1.66753	2.03754	2.28303	2.47566	2.63950	2.77618

2.24213

Table 4: The direct and indirect gap energies of the InN, InP, and InN_{0.50}P_{0.50} compounds at different pressure values with TR-mBJ approach.

Table 5: The hydrostatic pressure coefficients, α and β for the cubic InN, InP, and InN_{0.50}P_{0.50} compounds.

2.36479

 $E_{\Gamma \to X}$

Compounds	Band gap (TB-mBJ)	α (10 ⁻² eV/GPa)	<i>B</i> (10 ⁻⁴ eV/GPa)
InN	$E_{\Gamma \to \Gamma}$	2.03, 2.54ª	-2.39, -1.51ª
	$E_{\Gamma \to X}$	$0.51, 0.59^{a}$	$-0.36, -0.53^{a}$
$InN_{0.50}P_{0.50}$	$E_{\Gamma \to \Gamma}$	2.34	-4.91
	$E_{\Gamma \to X}$	-0.14	-0.42
InP	$E_{\Gamma o \Gamma}$	6.97, 7.81 ^a	-10.7, -10.53 ^a
	$E_{\Gamma o X}$	$-2.61, -2.09^{a}$	2.51, 1.65ª

aRef. [43].

Results obtained using this approach are closed to the available experimental data. The calculated band structures of the InN_vP_{1-v} compounds at different composition x = (0.00, 0.25, 0.50, 0.75, 1.00), within the TB-mBJ approximation, are shown in Figure 4.

Our calculations allow us to notice that the considered compounds are semiconductors in the range of all concentrations with a direct band gap of about 0.79, 0.87, and 1.66 eV, for the InN, InN_{0.5}P_{0.5}, and InP, respectively. These values confirm the importance of these compounds for the design and analysis of various optoelectronic and photonic devices.

Results obtained here for the direct band gap $(\Gamma \rightarrow \Gamma)$ and indirect one $(\Gamma \rightarrow X)$, for each concentration x, are reported in Table 2. It is clearly seen that the InN_vP_{1-v} direct band gap $(E_{r \rightarrow r})$ increases when composition x decreases and can be explained by the effect of N-dopant on the decrease in lattice parameter and also the presence of new energy bands in the material. Inversely, the indirect $(E_{\Gamma \to Y})$ band gap decreases with the P-dopant augmentation.

Moreover, the variation curves versus composition xof each band gap $(E_{\Gamma \to \Gamma}, E_{\Gamma \to X})$ undergo a simple polynomial quadratic fit and are shown in Figure 5. The InN_xP_{1-x} bowing factor values of the energy gap is found to be 1.5625 and -0.5007 eV for direct and indirect transitions, respectively.

2.02815

The equations of fitted curves of the InN_vP_{1-v} direct and indirect band gaps are given by the following equations:

$$E_{\Gamma \to \Gamma} = 1.587 - 2.2936x + 1.5625x^2 \tag{4}$$

1.94413

$$E_{r \to x} = 2.4411 + 2.0475x - 0.5007x^2 \tag{5}$$

3.3 Density of States

The density of states tells us how many states per unit energy exist in the vicinity of a certain energy level.

Figure 6 shows the total and the partial densities of states of InN, InP, and InN_{0.5}P_{0.5} alloys, respectively. They were calculated using the plane wave-local density approximation (PW-LDA). It can be seen from Figure 6a that the valence band comprises two regions, a lower (LVB) and upper (UVB) bands, respectively. For the InN compound, the In-4d and N-2s states are dominant in the LVB, with a high contribution of In-4d states, while the UVB is dominated by In-5s states, with a little contribution of In-5p and N-2s states. The conduction band (CB) is essentially populated by In-5s, In-5p and N-2p states.

It is seen from Figure 6b that the In-4d and P-3s orbital contribute to the UVB of the DOS in InP binary compound. The uppermost part of the valence band is dominated of the In-5p and P-3p states, with a small contribution of In-4d states. The CB is formed of a mixture of all states, with a high contributions of the In-5s and P-3p orbitals.

It is observed from Figure 6c that in the InN_{0.50}P_{0.50} ternary alloy, the LVB is mainly populated by In-4d, N-2s

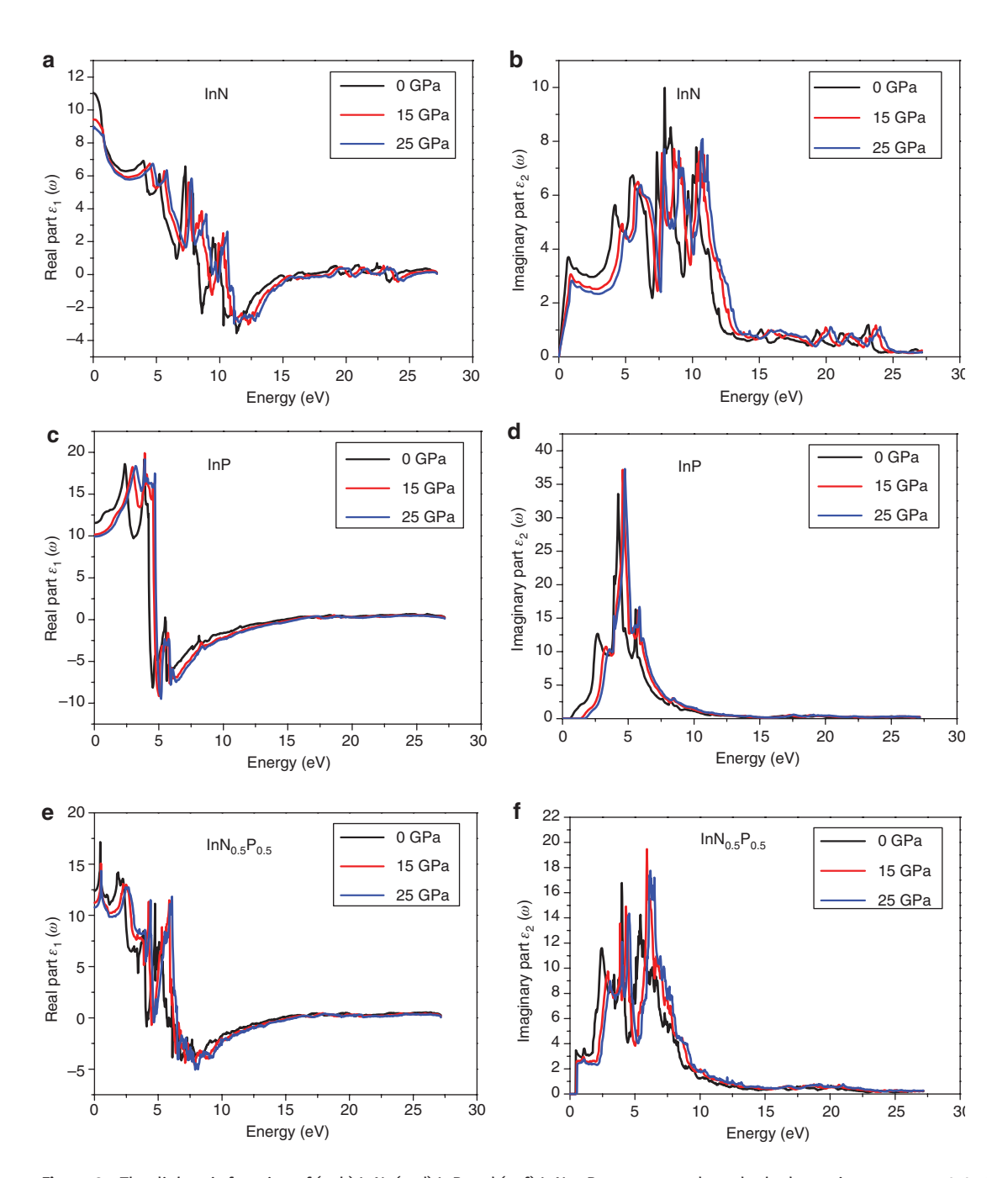


Figure 9: The dielectric function of (a, b) InN, (c, d) InP and (e, f) $InN_{0.50}P_{0.50}$ compounds under hydrostatic pressure at 0.0, 15, and 25 GPa.

and P-3s states. The UVB is essentially formed by In-5s and a mixture of In-5p, N-2p and P-3p states. The CB results from a mixture of In-5s, In-5p, and a small contribution of N-2p and P-3p states.

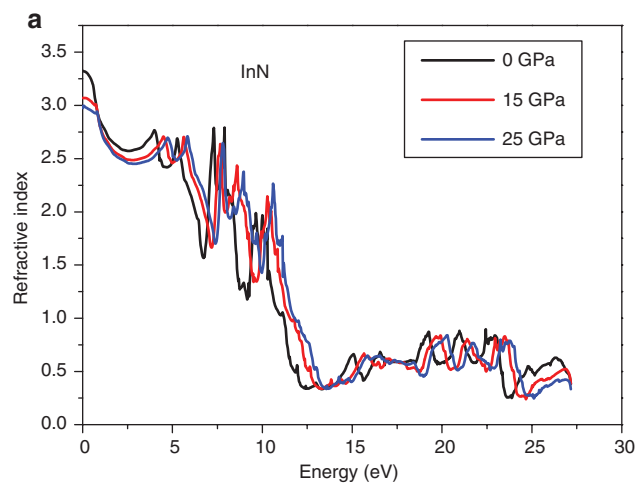
4 Optical Properties

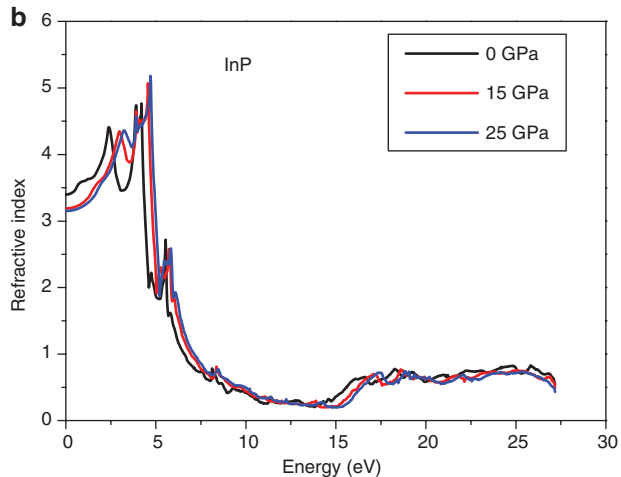
In order to investigate the optical properties of the ternary alloys ${\rm InN_{_y}P_{_{1-y}}}$, we have studied all the possible transitions

between valence and CBs. The frequency-dependent dielectric functions $\varepsilon_1(\omega)$ and $\varepsilon_2(\omega)$ [34], the real and imaginary parts of the complex dielectric function $\varepsilon(\omega)$ are given by the following equations:

$$\varepsilon_1(\omega) = 1 + \frac{2}{\pi} P \int_0^\infty \frac{\omega' \varepsilon_2(\omega')}{{\omega'}^2 - {\omega'}^2} d\omega'$$
 (6)

In the imaginary part $\varepsilon_{2}(\omega)$, the momentum dipole elements





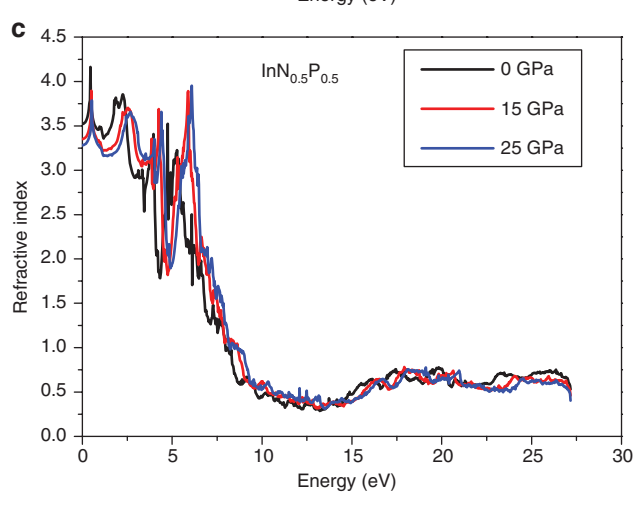


Figure 10: The refractive index of (a) InN, (c) $InN_{0.50}P_{0.50}$, and (b) InP compounds under hydrostatic pressure at 0.0, 15, and 25 GPa, respectively.

$$M_{cv}(k) = \langle u_{vk} | \delta \nabla | u_{ck} \rangle \tag{7}$$

describes the direct transitions between the valence band and the CB u_{vk} and u_{ck} states, respectively, with δ as a unit

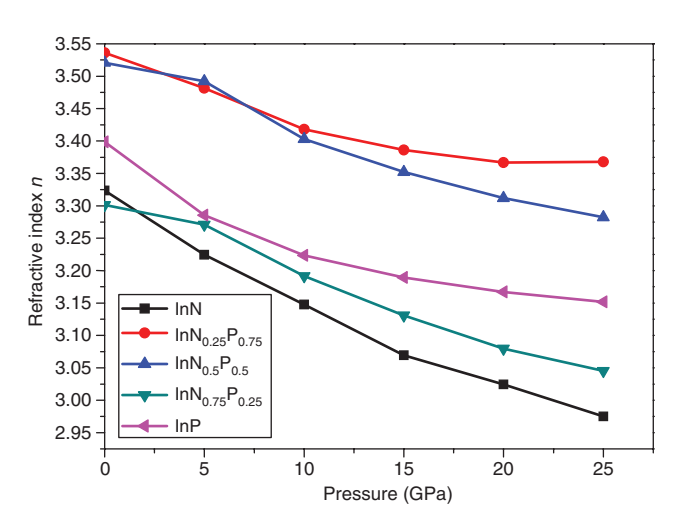


Figure 11: The refractive indices variation versus pressure of the $InN_{\nu}P_{\nu}$ alloys at different composition of x.

vector defining the electric field. The integral is carried out over the first Brillouin zone.

On the other hand, *P* designates that the integral is to be evaluated in the principal value sense in the real part $\varepsilon_{\bullet}(\omega)$. This latter can be calculated from imaginary part by means of the Kramers-Kronig transformation [35].

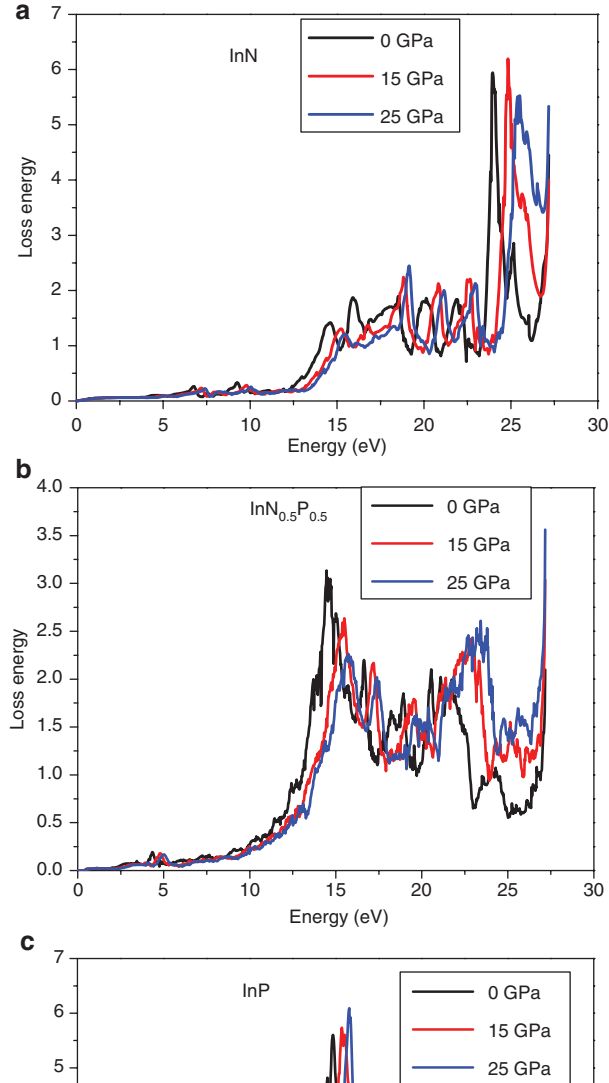
The spectral variations of the dielectric function $\varepsilon(\omega)$ within the real and imaginary parts for the InN, InP compounds, and their related ternary InN_vP_{1-v} alloy at the composition x = 0.5 are shown in Figure 7.

From the variation curves of the imaginary part of the dielectric function $\varepsilon_{2}(\omega)$ according to the energy, which reflects the absorption of the material. We can get different direct interband transitions. The main peaks of the structure are visible at 3.70, 5.63, 7.6, and 9.98 eV which correspond well to the InN compound at energies 0.72, 4.20, 7.33, 7.93 eV, respectively. These peaks may belong to the electronic direct transition from In-3p states to In-4s and N-2p states as predicted by Usman et al. [36]. The peak around 7.33 eV is attributed to 3p, 4s valence states of Indium to N-2p and In-4s [36]. Whereas, the peak at 9.98 eV is related to mixed transitions.

For the InP alloy, we observe two peaks located at 2.73 and 4.23 eV. We have to note that our calculated peak positions are much closer to Feng et al. data (3.06, 4.69 eV) [37] than the calculated values (2.40, 4.10 eV) [38] using the FPLMTO method. The first peak corresponds mainly to the interband direct transitions from the top of valence bands to the bottom of CBs.

The maximum of absorption is located at 9.98, 33.55, and 16.76 eV for InN, InP, and InN_{0.5}P_{0.5}, respectively.

Moreover, we have calculated the refractive index $n(\omega)$ using the following relation:



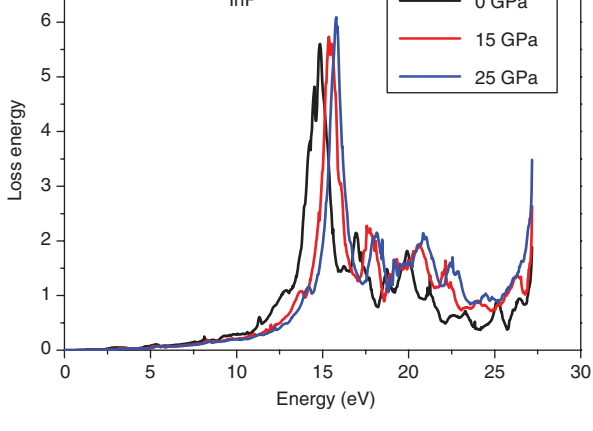


Figure 12: Energy loss of (a) InN, (c) InP, and (b) InN_{0.50}P_{0.50} compounds under pressure of 0.0, 15, and 25 GPa, respectively.

$$n(\omega) = \left[\frac{\varepsilon_1(\omega)}{2} + \frac{\sqrt{\varepsilon_1^2(\omega) + \varepsilon_2^2(\omega)}}{2}\right]^{1/2}$$
 (8)

Other models were used to calculate the refractive index $n(\omega)$ for comparison and confirmation of results. These models are presented as follow:

Moss model [39]:

$$n^4 E_g = 95 \text{ eV}$$
 (9)

where n and $E_{\rm g}$ are, respectively, the refractive index and the energy gap.

Ravindra model [39]:

$$n=4.084-0.62 E_{\alpha}$$
 (10)

Herve-Vandamme model [39]:

$$n^2 = 1 + \left(\frac{A}{E_{\rm g} + B}\right)^2 \tag{11}$$

where A is the hydrogen ionisation energy 13.6 eV and B=3.47 eV is a constant presumed to be the difference between the UV resonance energy and the band gap E_a .

Reddy model [39]:

$$n^4(E_g - 0.365) = 154 \tag{12}$$

Kumar and Singh model [39]:

$$n = KE_g^c \tag{13}$$

where K = 3.3668 and C = -0.32234.

The static values of the refractive index $n(\omega)$ for $\omega=0$ are listed in Table 3. As can be seen from Figure 10, the refractive index $n(\omega)$ decreases when increasing the nitrogen composition x. The values obtained here are also computed using different models (8–12), cited above, for the validation and comparison purposes. Results agree well between these models.

5 Hydrostatic Pressure Effect

When a material is destined for a technological application, it becomes necessary to study the comportment of the material under external disturbances such as pressure, temperature, electric field, and magnetic field. In this article, we have chosen to study the hydrostatic pressure on the energy gaps and the optical properties.

Variations of band gap energies and optical properties under hydrostatic pressure were calculated using the FP-LAPW methods within LDA and TB-mBJ approach, respectively. Firstly, we have calculated the lattice constant values as a function of pressure at *P* equal to 0, 5, 10, 15, 20, and 25 GPa, using the following formula [42]:

$$a(P) = a(0) \left[1 + \left(\frac{B'}{B} \right) P \right]^{\left(\frac{-1}{\varepsilon B'} \right)^2}$$
 (14)

where *B* is the bulk modulus, *B'* the pressure derivative of the bulk modulus, and a(P) the lattice parameter at the indicated pressure P.

The direct and indirect band gap energies of the InN_vP_{1-v} at x = 0.00, 0.50, and 1.00 compositions were computed and plotted in Figure 8.

When the applied pressure is increased, a small variation for both gap energies is observed with an increase in the direct band gap $E_{\Gamma \to \Gamma}$ and a decrease in the indirect band gap $E_{\Gamma \to X}$, and that is due to the decrease of the lattice constant (volume compression). We can also notice that the InP compound changes character from a direct to an indirect band gap semiconductor at $P \ge 7.80$ GPa. The direct and indirect band gap energy values are listed in Table 4. Furthermore, we have fitted our results to a quadratic function as given in the empirical formula [42]:

$$E_{g}(P) = E_{g}(0) + \alpha P + \beta P^{2}$$

$$\tag{15}$$

where $E_{\nu}(0)$ represents the band gap energy at zero pressure, P is the pressure in GPa, α and β are the first- and second-order pressure coefficients, respectively. The pressure coefficients α and β obtained from the fitted curves of the cubic InN and InP binary compounds as well as the $InN_{0.50}P_{0.50}$ ternary alloy are summarised in Table 5. Results obtained here are compared to the available data where a good agreement is observed for binary constituents. We have to note that we have not found any report in literature for comparison.

We reported on the optical properties under different values of pressure for InN, InP, and InN_{0.50}P_{0.50} alloys. The dielectric functions versus photon energy and the behaviour of refractive indices at various hydrostatic pressures were investigated and shown in Figures 9 and 10, respectively. We can see the similarity of spectra of the dielectric function under different values of pressure except of a slight shift explained by the effect of pressure on the band energies. On the other hand, the refractive index decreases slightly due to the condensation of atoms and compression of the unit cell volume. It is clearly seen from Figure 10a-c that the refractive index decreases dramatically versus pressures for the InN compound. For the second binary compound InP, we observe a decrease in the value of the refractive index versus pressure. The maximum of the value of the refractive index is found to be equal to 5.4 and observed at the energy value of 4.85 eV. The refractive index of the ternary alloy $InN_{0.50}P_{0.50}$ obeys

to the same behaviour and the maximum of the refractive index is 4.24 and it is located at the energy value of 0.5 eV. Roughly, the pressure presents no significant effect and this confirms the stability of optical properties of our material.

In Figure 11, we present both the effect of the pressure and the nitride composition on the refractive index. The examination of the curve given in Figure 11 shows that the refractive index decreases upon increasing the pressure in the considered range and the same observation when regarding the composition increasing.

Knowing that the energy loss function is a primordial tool for the investigation of different aspects of materials [44]. Electron energy loss function for InN, InP, and $InN_{0.50}P_{0.50}$ under pressure are depicted in Figure 12. We observe from this figure that for a photon with energy lesser than the band gap of the considered compound no energy loss occurs and this means no scattering happens. In the intermediate energy range, inelastic scattering is observed and the loss energy value is maximal. The major peaks for a pressure equal to zero are located at 23.82, 14.61, and 13.90 eV for InN, InP, and the $InN_{0.50}P_{0.50}$, respectively. These peaks in the energy loss spectrum are shifted to higher energy under pressure and correspond to plasma resonance and the corresponding frequency is the plasma frequency.

6 Conclusion

The structural, electronic, and optical properties of zincblende InN, InP, and InN, P1-x solid solutions have been carried out using the FP-LAPW method within DFT theory. We have considered the effect of pressure variations on the direct and indirect energy band gaps and optical properties of the InN, InP, and InN_vP_{1-v} compounds. The conclusions drawn from this study are as follows:

- (i) The lattice constant of the InN_xP_{1-x} decreases when increasing the concentration of nitride and the bulk modulus increases with the increase in the concentration x.
- (ii) The direct energy band gaps decrease upon increasing the nitride composition x. The InN_xP_{1-x} presents a direct band gap for all composition *x*.
- (iii) In the considered pressure range, the ternary alloy InN_vP_{1-v} presents direct band gap energy for each composition and we observe a small increasing for both direct and indirect band gap energies versus pressure.
- (iv) Under pressure, the structures of the optical parameters of both binary compounds and their ternary InN_vP_{1-v} solid solution present a good optical stability.

References

- [1] L. Ley, R. A. Pollak, F. R. McFeely, S. P. Kowalczyk, and D. A. Shirley, Phys. Rev. B 9, 600 (1974).
- [2] D. E. Aspnes and A. A. Studna, Phys. Rev. B 27, 985 (1983).
- [3] C. M. Herzinger, P. G. Snyder, B. Johs, and J. A. Woollam, J. Appl. Phys. 77, 1715 (1995).
- [4] A. G. Bhuiyan, A. Hashimoto, and A. Yamamoto, J. Appl. Phys. 94, 2779 (2003).
- [5] J. Wu, W. Walukiewicz, K. M. Yu, J. W. Ager III, E. E. Haller, et al., Appl. Phys. Lett. 80, 3967 (2002).
- [6] Z. Boussahla, B. Abbar, B. Bouhafs, and A. Tadjer, J. Solid State Chem. B 178, 2117 (2005).
- [7] A. Ben Fredj, M. Debbichi, and M. Said, Microelectronic J. 38, 860 (2007).
- [8] K. H. Hellwege and O. Madelung, Landolt- Bornstein, Semiconductors: (Physics of Group IV Elements and III-V Compounds). New Series, Group III, 17, Pt. a Springer Verlag, Berlin 1982, p. 602.
- [9] M. Kondow, T. Kitatani, S. Nakatsuka, M. C. Larson, K. Nakahara, et al., IEEE J. Sel. Top. Quant. Elect. 3, 719 (1997).
- [10] M. Kondow, T. Kitatani, M. C. Larson, K. Nakahara, K. Uomi, et al., J. Cryst. Growth 188, 255 (1998).
- [11] D. J. Friedman, J. F. Geisz, S. R. Kurtz, D. Myers, and J. M Olson, J. Cryst. Growth 195, 409 (1998).
- [12] S. R. Kurtz, A. A. Allerman, E. D. Jones, J. M. Gee, J. J. Banas, et al., Appl. Phys. Lett. 74, 729 (1999).
- [13] L.-W. Wang, L. Bellaiche, S.-H. Wei, and A. Zunger, Phys. Rev. Lett. 80, 4725 (1998).
- [14] A. Lindsay and E. P. O'Reilly, Solid State Commun. 112, 443 (1999).
- [15] M. Aslan, A. H. Reshak, B. G. Yalcin, S. Bagci, and M. Ustundag, Philos. Mag. 96, 991 (2016).
- [16] S. M. Sze, Physics of Semiconductor Devices, Wiley, New York 1981.
- [17] P. Blaha, K. Schwarz, G. K. H. Madsen, D. Kvasnicka, J. Luitz, Wien2k, An Augmented Plane Wave Plus Local Orbital Program for Calculating Crystal Properties, Vienna University of Technology, Vienna, Austria 2001.
- [18] K. Schwarz and P. Blaha, Comput. Mater. Sci. 28, 266 (2003).
- [19] F. D. Murnaghan, Proc. Natl. Acad. Sci. U.S.A. 30, 244 (1944).

- [20] D. Koller, F. Tran, and Blaha, Phys. Rev. B 85, 1-8 (2012).
- [21] H. Shi and Y. Duan, Phys. Lett. A373, 165 (2008).
- [22] A. Abdiche, H. Abid, R. Riane, and A. Bouaza, Acta Phys. Poloni. A 117, 924 (2010).
- [23] M. I. Ziane, B. Zouaoui, T. Ouhrni, and B. Hamza, Mater. Sci. Semiconduct. Proc. 30, 181 (2015).
- [24] J. Serrano, A. Rubio, E. Hernandez, A. Munoz, and A. Mujica, Phys. Rev. B 62, 16612 (2000).
- [25] R. Ahmed, S. J. Hashem Far, H. Akbarzadeh, M. Ahmed, and F. E. Aleem, Comput. Mater. Sci. 39, 580 (2007).
- [26] S. Q. Wang and H. Q. Yes, Phys. Rev. B 66, 235111 (2002).
- [27] W. Shen and A. Zunger, Phys. Rev. B 60, 5404 (1999).
- [28] M. Guemou, B. Bouhafs, A. Abdiche, R. Khenata, Y. Al Douri, et al., Physica B 407, 1292 (2012).
- [29] L Vegard, Zeitschrift Fur Physik 5, 17 (1921).
- [30] F. Bechstedt and R. Del Sole, Phys. Rev. B 38, 7710 (1988).
- [31] D. Jenkins, Properties of Group III-Nitrides (Ed. J. H. Edgar), EMIS Data Reviews 11, INSPEC, London 1994, p. 10233.
- [32] P. Rochon and E. Fortin, Phys. Rev. B 12, 5803 (1975).
- [33] O. Madelung and M. Schulz, Londolt-Bornstein: numerical data and functional relationships in science and technology. Cryst Solid State Phys, 17a. Springer-Verlag, Berlin 1987.
- [34] S. Adachi, Properties of Semiconductor Alloys: Group-IV, III-V and II-VI Semiconductors, John Wiley & Sons, Ltd., UK 2009,
- [35] T. Ouahrani, A. H. Reshak, R. Khenata, B. Amrani, M. Mebrouki, et al., J. Solid State Chem. 183, 46 (2010).
- [36] Z. Usman, C. Cao, and T. Mahmood, Physica B 430, 67 (2013).
- [37] Z. Feng, H. Hu, S. Cui, and W. Wang, Physica B: Condensed Matter 404, 2103 (2009).
- [38] R. Ahuja, S. Auluck, O. Eriksson, J. M. Wills, and B. Johansson, Solid State Commun. 104, 249 (1997).
- [39] S. K. Tripathy, Opt. Mater. 46, 240 (2015).
- [40] S. Berrah, Phys. Scr. 75, 414 (2007).
- [41] S. K. Tripathy, Opt. Mat. 46, 240 (2015).
- [42] S. Adachi, Properties of Group III-V and II-VI Semiconductors, Wiley, New York 2005, (Chapter 2).
- [43] P. E. Van Camp, V. E. Van Doren, and J. T. Devreese, Phys. Rev. B 41, 1598 (1990).
- [44] S. Loughin, R. H. French, L. K. Noyer, W. Y. Ching, and Y. N. Xu, J. Phys. D 29, 1740 (1996).